IEEE Open Journal of the Communications Society

Received 24 July 2024; accepted 7 August 2024. Date of publication 14 August 2024; date of current version 30 August 2024.

Digital Object Identifier 10.1109/OJCOMS.2024.3444719

Noncoherent Frequency-Shift Keying for Ambient Backscatter Over OFDM Signals

MOHAMED A. ELMOSSALLAMY [1] (Member, IEEE), MIAO PAN [1] (Senior Member, IEEE), RIKU JÄNTTI [2] (Senior Member, IEEE), KARIM G. SEDDIK [3] (Senior Member, IEEE), GEOFFREY YE LI [4] (Fellow, IEEE), AND ZHU HAN [1,5] (Fellow, IEEE)

[1]Electrical and Computer Engineering Department, University of Houston, Houston, TX 77004, USA

[2]Department of Communications and Networking, Aalto University, 02150 Espoo, Finland

[3]Electronics and Communications Engineering Department, American University in Cairo, New Cairo 11835, Egypt

[4]Department of Electrical and Electronic Engineering, Imperial College London, SW7 2AZ London, U.K.

[5]Department of Computer Science and Engineering, Kyung Hee University, Seoul 446-701, South Korea

CORRESPONDING AUTHOR: M. A. ELMOSSALLAMY (e-mail: m.ali@ieee.org)

This work was supported in part by NSF under Grant CNS-2107216, Grant CNS-2128368, Grant CMMI-2222810, and Grant ECCS-2302469; in part by the U.S. Department of Transportation; in part by Toyota; in part by Amazon; and in part by the Japan Science and Technology Agency (JST) Adopting Sustainable Partnerships for Innovative Research Ecosystem (ASPIRE) under Grant JPMJAP2326.

ABSTRACT In this paper, we investigate frequency shift keying (FSK) over ambient orthogonal frequency division multiplexed (OFDM) signals. By cycling through a sequence of antenna loads providing different phase shifts at the tag, we are able to unidirectionally shift the ambient OFDM spectrum either up or down in frequency to disjoint subsets of the subcarriers allowing the implementation of FSK. We exploit the guard bands and the orthogonality of the OFDM subcarriers to avoid both direct-link and adjacent channel interference. Different from energy detection based techniques that suffer from asymmetric error probabilities and rely on signal-to-noise ratio (SNR) dependent detection thresholds, the proposed scheme has symmetric error probabilities and allows simple detection without the need for a threshold. We present both binary and four-ary schemes, and analyze the error performance of the optimal noncoherent detectors. For the binary scheme, we obtain exact expressions for the average probability of error, while for the four-ary scheme, a union bound is used to characterize the error performance. Single and multi-antenna receivers are considered, and their performance is analyzed. Finally, we present simulation results to corroborate our analysis and investigate the effects of multiple system parameters. The results show that the proposed scheme outperforms the baseline energy detection based schemes available in the literature in various scenarios by up to 5 dB.

INDEX TERMS Ambient backscatter, Internet of Things, green communications, performance analysis, OFDM.

I. INTRODUCTION

FUTURE Internet of Things (IoT) networks are envisioned to possess billions of devices, many of whom will be severely constrained in cost and power. To realize this vision, new low-cost and energy-efficient communication techniques are needed. Backscatter radio is one of the main contenders to meet this fierce demand for connectivity. In traditional backscatter radio systems [1], [2], ultra-low power devices, commonly referred to as tags, are able to communicate by merely connecting their antennas to different loads to reflect and phase shift impinging RF signals to a reader device. Therefore, all power-hungry signal processing is consolidated in the reader, allowing ultra-low-power tags without power-hungry active RF components, e.g., analog-to-digital converters (ADCs) and power amplifiers. However, traditional backscatter radio systems, e.g., RFID, require dedicated infrastructure to provide clean, constant illumination for tags to communicate.

To alleviate the need for dedicated infrastructure, it has been proposed in [3] to use the existing ambient RF transmission from traditional TV, WiFi, and cellular networks to illuminate backscatter tags. If we are able to piggyback information over ambient RF signals, then ubiquitous ultra-low-power radio communication is within reach since RF transmissions are omnipresent [4]. However, using already modulated RF signals for backscatter poses many challenges.

Over the last few years, many signaling techniques for ambient backscatter have been proposed. Early prototypes in [3], [5], [6], [7], [8] proved ambient backscatter is a viable technology. In [3], ambient TV transmissions have been exploited to establish a link between two battery-less tags. By backscattering at a much lower rate than the high bandwidth TV signal, a simple averaging detector has been used to decode the tag's information. Improved bit rates and communication range have been achieved in [5] by mitigating the interference coming directly from the ambient source and using more robust orthogonal spread spectrum signaling. In [6], bi-directional Internet connectivity has been achieved between a tag and a commercial off-the-shelf WiFi device. This has been enabled by received signal strength indicator (RSSI) measurements in the uplink, and energy detection of short WiFi packets in the downlink. In [7], coherent phase-shift keying has been used, enabled by a modified full-duplex-capable WiFi access point (AP) that is able to cancel direct link interference and estimate the channel. In [8], Bluetooth and WiFi signals have been shifted to the two adjacent channels using rapid On-off Keying (OOK) and have been received using commodity radios. Furthermore, it has been shown in [9], [10], [11] that packets for multiple standards can be generated via backscatter. In [9], it has been shown that WiFi packets can be generated by backscattering modified Bluetooth packets. While in [10] and [11], respectively, FM signals and LoRa signal have been generated by backscattering ambient signals of the same modulation. In [12], three techniques based on controlling tag impedance switching frequency have been proposed. The proposed techniques avoided direct-link interference by translating the backscattered signals out of the ambient signal bandwidth and a prototype demonstrated a communication range of up to 26m, consuming only 24 μW for transmission. Mitigation of direct-link interference in a cognitive cloud radio access (C-RAN) has been investigated in [13], where a centralized cloud processor with perfect knowledge of the primary ambient signal, and the received signal at the reader can subtract the contribution of the direct-link. Lastly, in [14], the integration of backscatter devices into the LTE downlink is explored. The study proposed the use of frequency shifting at the tag to introduce an artificial Doppler shift, which can be detected by the receiver's channel estimator.

Motivated by the promising early prototypes, a slew of research investigated more theoretical aspects of ambient backscatter communications, such as modeling, error performance and capacity analysis [15], [16], [17], [18], [19], [20], [21]. It has been shown in [15] that adding backscattering nodes to a legacy MIMO communication system increases the achievable sum rate. The performance of the differential encoding and averaging detection scheme originally proposed in [3] has been investigated in the case of a single antenna at the reader in [16] and multiple antennas in [17]. More research focusing either on noncoherent or semi-coherent detection performance of ambient backscatter can be found in [18], [19], [22]. Most of the aforementioned works assume no specific modulation for the ambient source and rely heavily on Gaussian approximations.

Since most current wireless systems rely on orthogonal frequency division multiplexing (OFDM), there have been some efforts to exploit the structure of the OFDM waveform to provide more robust ambient backscatter communications. In [21], the remaining part of the cyclic prefix has been used to cancel direct-link interference. While in [23], the orthogonality of the OFDM subcarriers has been exploited to avoid direct link interference by shifting backscattered energy to null subcarriers. The two aforementioned schemes rely on energy detection and suffer from asymmetric error performance and cumbersome threshold estimation; however, they don't require any knowledge of the relevant channels. In [24], the authors proposed the use of a bank of notch filters at the tag to selectively block certain subcarriers and analyzed detection performance under perfect knowledge of direct and backscatter channels. However, the implementation of the required bank of notch filters may prove impractical, especially in a passive tag. In [25], the authors assumed certain OFDM symbols contain only known pilot signals and studied two coherent backscatter schemes over these known symbols relying on phase shifter and delay circuits. More recently, in [26], special backscatter sequences have been proposed to enable phase shift keying (PSK) while maintaining orthogonality with the ambient OFDM signal by reserving some subcarriers for the backscattering. In [27], a prototype utilizing both (PSK) and frequency shifting has been developed to demonstrate that information from multiple tags can be jointly detected by exploiting subcarrier redundancy, i.e., the wide bandwidth of an OFDM system. Finally, it is worth mentioning that it has been shown in [28] that ambient backscatter can generally benefit legacy OFDM transmissions by offering a form of channel diversity.

In this paper, we investigate frequency shift keying over ambient OFDM signals extending our previous work presented in [29]. Our contributions in this paper can be summarized as follows:

- We propose a backscatter technique that allows binary frequency shift keying modulation over ambient OFDM carriers. Different from other frequency shifting techniques that rely on energy detection on adjacent channels on both sides of the ambient signal, e.g., [30], we propose a frequency shifting technique that relies on cycling through the phase shifts of a complex sinusoid in both directions, allowing unidirectional frequency shift either up or down in frequency and enabling the use of frequency-shift keying.

- We analyze the optimal noncoherent detector and obtain an exact expression for the average probability of error. Different from schemes that rely on energy detection [21], [23], [24], our optimal detector has symmetric error probabilities for '0's and '1's and does not require the estimation of a signal-to-noise-ratio (SNR) dependent threshold.
- We propose a 4-ary modulation scheme to increase the communication rate. The proposed 4-ary builds on the same basic idea of the binary scheme and retains all of its advantages, such as symmetric error probabilities and easy detection without a threshold. Furthermore, we analyze the error performance and derive an upper bound for the average error probability.
- We propose the use of noncoherent receive combining techniques when multiple antennas are available at the receiver. We investigate the distribution of the SNR at the output of the combiner and derive an expression for the average probability of error. The proposed combining techniques are easy to implement and drastically improve performance.
- We provide simulation results to verify our analysis and study the effects of system parameters, namely, the maximum channel delay spread and OFDM symbol size, on the error performance. Our results show the proposed scheme outperforms energy detection based schemes in [21], [23], [30].

The rest of the paper is organized as follows. In Section II, we outline our system model. In Section III, we introduce the proposed binary ambient backscatter modulation scheme, study the optimal detector, and analyze the error performance. In Section IV, we introduce the proposed four-ary modulation scheme, investigate the optimal detector, and analyze its error performance. In Section V, we extend our analysis to the multi-antenna receiver case for both the binary and four-ary schemes. In Section VI, we provide simulation results to verify our analysis and benchmark our proposed schemes against existing schemes in the literature. Finally, we conclude the paper in Section VII.

II. SYSTEM MODEL

We consider the classical three-node ambient backscatter system model similar to the one used in [21], [23], [30], and shown in Fig. 1. In general, ambient backscatter communications rely on RF transmissions generated by an existing traditional communication system, hereinafter referred to as the *legacy* communications system. We assume the legacy communication system employs OFDM, e.g., LTE or WiFi. The legacy communication nodes possess traditional active transceivers powered by large capacity batteries or connected to the power grid, and thus are unaffected by the weaker backscattered signals. On the other hand, the ambient backscatter communication system consists of ultra-low-power tags that communicate by changing their antenna loads to backscatter ambient signals back to a reader device. The tags typically rely only on energy harvesting to support their operation [4], while the reader is a traditional radio transceiver.

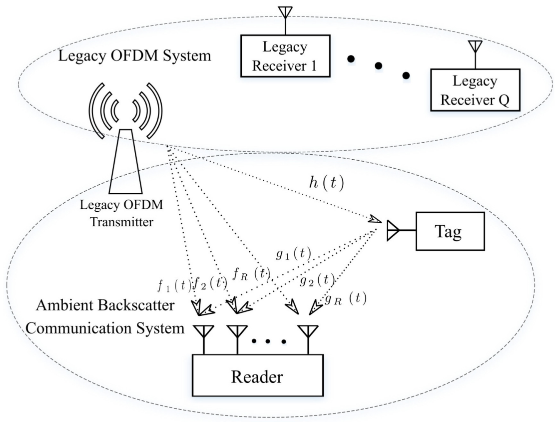

FIGURE 1. The system model.

Assume there are one ambient source and one tag with a single-antenna each, and one reader with up to R antennas. All channels are assumed to be mutually independent multipath Rayleigh fading channels. Let $f_r(t)$, $h(t)$ and $g_r(t)$ denote the channel impulse responses between the ambient source and the reader's r-th antenna, the ambient source and the tag, and the tag and the reader's r-th antenna, respectively. The corresponding delay spreads are given by τ_f, τ_h and τ_g, assuming the delay spread observed at the reader is the same across all its antennae.

The bandpass signal emitted from the legacy transmitter can be written as

$$s(t) = \Re\left\{\sqrt{\rho}\ s_l(t)e^{j2\pi \mathsf{f_c} t}\right\}, \tag{1}$$

where $\Re\{\cdot\}$ denotes the real-part operator, ρ is the average transmitted power, $s_l(t)$ is the baseband representation of $s(t)$, and $\mathsf{f_c}$ is the carrier center frequency. Hence, the signal received at the tag is given by

$$x(t) = \Re\left\{\left[\sqrt{\rho}\ s_l(t) * h_l(t)\right]e^{j2\pi \mathsf{f_c} t}\right\}, \tag{2}$$

where $*$ denote linear convolution, and $x_l(t) = \sqrt{\rho}s_l(t)*h_l(t)$ is the baseband representation of $x(t)$.

The tag modulates its information by simply connecting its antenna to different loads. Hence, no thermal noise is added at the tag [16], [17], [21]. Let $b_l(t)$ denote the baseband representation of the tag's modulation waveform with corresponding bandpass signal $b(t)$ and α denote the tag reflection coefficient. The path-loss attenuation for the backscattered and direct links is denoted by β^b and β^d, respectively. Hence, the received signal at the reader's r-th antenna can be written as

$$y_r(t) = \underbrace{\sqrt{\beta^b}[\alpha x(t)b(t)] * g_r(t)}_{y_r^b(t)} + \underbrace{\sqrt{\beta^d} s(t) * f_r(t)}_{y_r^d(t)} + w_r(t), \quad (3)$$

where $y_r^b(t) = [\alpha x(t)b(t)] * g_r(t)$ is the signal backscattered from the tag and received at the r-th receiver antenna, $y^d(t) = s(t) * f_r(t)$ is the signal received directly from the legacy transmitter at the r-th receiver antenna, and $w_r(t)$ is bandpass Gaussian noise at the r-th receiver antenna, which is independent of both $y_r^b(t)$ and $y_r^d(t)$ for all $r \in \{1, 2, \ldots, R\}$. Note that tag's information in present only in the term $y_r^b(t)$, while $y_r^d(t)$ is the direct-link, i.e., legacy-transmitter to reader, interference. The baseband representation of the received signal at the r-th antenna can be written as

$$y_{r,l}(t) = y_{r,l}^b(t) + y_{r,l}^d(t) + w_{r,l}(t), \quad (4)$$

where $y_{r,l}^b(t)$, $y_{r,l}^d(t)$, and $w_{r,l}(t)$ denote the baseband representations of $y_r^b(t)$, $y_r^d(t)$, and $w_r(t)$, respectively.

At the reader, the received signal is down-converted to baseband and passed through an analog-to-digital converter (ADC). Let N_f denote the number of subcarriers, or equivalently the length of the fast Fourier transform (FFT), and N_{cp} denote the cyclic prefix length. The resultant discrete-time baseband sequence at the r-th receive antenna for one OFDM symbol can be written as

$$y_{r,l}[n] = y_{r,l}^b[n] + y_{r,l}^d[n] + w_{r,l}[n], \quad n = 1, 2, \ldots, N_f + N_{cp}, (5)$$

where $w_{r,l}[n]$ is complex baseband additive white Gaussian noise (AWGN) with zero-mean and variance σ_w^2 at the r-th reader antenna. Let $h_l[n]$, $f_{r,l}[n]$, and $g_{r,l}[n]$ denote the discrete-time baseband representation of $h(t), f_r(t)$, and $g_r(t)$, respectively, whose lengths are given by $L_h = \lfloor \tau_h \mathsf{f_s} \rfloor$, $L_f = \lfloor \tau_f \mathsf{f_s} \rfloor$, and $L_g = \lfloor \tau_g \mathsf{f_s} \rfloor$, where $\mathsf{f_s}$ is the sampling frequency. Let $\tau \triangleq \max\{\tau_f, \tau_h + \tau_g\}$ denote the maximum channel delay spread; hence, $L \triangleq \max\{L_f, L_h + L_g - 1\}$ denotes the discrete-time length of maximum channel delay spread. We assume channel lengths are the same for all reader's antennas. Moreover, in practice the tag-reader distance is fairly small and it is reasonable to assume $L_g = 1$ [21]. Then, we can write $y_{r,l}^b[n] = \alpha g_r x_l[n] b_l[n]$. In the rest of the paper, we use the discrete-time baseband model and drop the subscript l for notational convenience.

Our goal is to design the tag modulation to allow completely noncoherent detection of $b[n]$ from the received signals $\{y_r[n]\}_{r=1}^R$ without knowing either the transmitted OFDM symbol $s[n]$, the relevant channels $h[n]$, $\{f_r[n]\}_{r=1}^R$, and $\{g_r\}_{r=1}^R$ or even the average SNR.

III. TRANSCEIVER DESIGN AND PERFORMANCE ANALYSIS

In this section, we propose a frequency shift keying modulation scheme for backscatter communications over ambient OFDM signals. For ease of exposition, we describe the tag modulation waveform and study the optimal noncoherent detector for a single-antenna reader, i.e., $R = 1$, and leave the multi-antenna case to be presented in Section V. We also analyze the error performance of the proposed scheme and obtain an analytical expression for the average error probability.

A. TAG WAVEFORM DESIGN

In OFDM systems, several subcarriers along the edges of the spectrum, but still inside the channel bandwidth, are left null to serve as a guardband and satisfy FCC spectrum emission regulations. Recently, these guardbands have been proposed as one of the deployment options for narrowband IoT (NB-IoT) [31]. The number of those subcarriers will depend on the channel bandwidth and the subcarriers spacing. For example, a 10 MHz LTE waveform has 64 inband null subcarriers along the edges [32]. Let $\mathcal{U}$ and $\mathcal{L}$ denote the set of upper guard subcarriers and the set of lower guard subcarriers, respectively. “upper” refers to subcarriers above the center frequency and “lower” refers to subcarriers below the center frequency. In practice, the number of upper and lower subcarriers will be equal. Hence, we assume $|\mathcal{U}| = |\mathcal{L}| = N$, where $|\cdot|$ denote the cardinality of a set.

We design the tag modulation waveform to take advantage of these guardband subcarriers and the orthogonality inherent in the OFDM waveform to overcome direct-link interference while allowing simple square-law detection without an SNR dependent threshold. In particular, the tag modulation waveform selectively shifts the spectrum of the backscattered signal to either the upper or lower guardbands to transmit one bit of information. Hence, the detector can simply compare the energy in the two bands to decode the tag information. The detector does not need to know the transmitted OFDM symbol, any of the relevant channels, or even estimate a detection threshold. This scheme can be viewed as superimposing binary frequency-shift keying (BFSK) on top of the ambient signal. We propose a simple implementation that ensures no backscatter energy is shifted outside the channel bandwidth.

Similar to [21], [25], [28], [30], [33], we assume every backscatter symbol span the duration of one legacy OFDM symbol.[1] The tag uses the following waveform to convey one information bit per OFDM symbol,

$$b[n] \triangleq \begin{cases} e^{i2\pi \frac{N}{N_f} n}, & B = 0, \\ e^{-i2\pi \frac{N}{N_f} n}, & B = 1, \end{cases} \quad (6)$$

where $n = 1, 2, \ldots, N_f + N_{cp}$ and $B \in \{0, 1\}$ is the information bit being transmitted. Hence, as shown in Fig. 2, to transmit a ‘1’ bit, the tag will connect its antenna to

[1] Note that this assumption implies the backscatter device can achieve timing synchronization with the legacy OFDM transmission up to the cyclic-prefix length. We refer the reader to the discussion on synchronization in [30] for more details on how to achieve this synchronization. If synchronization is not achieved, the asynchronous mode in [30] can be applied to our proposed scheme at the cost of halving the transmission rate.

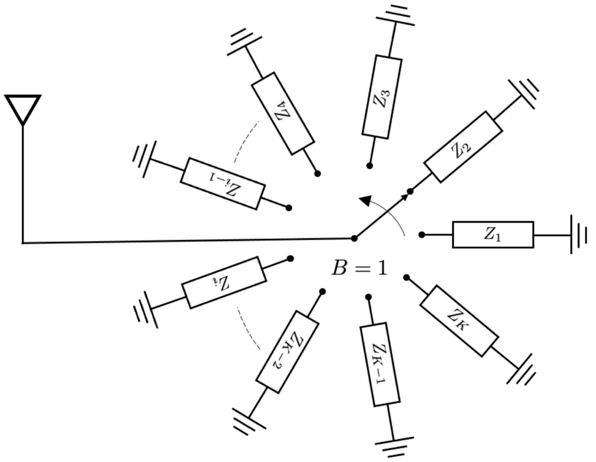

(a) Cycle through phase shifts, i.e., antenna's impedances, clockwise to send a '0'.

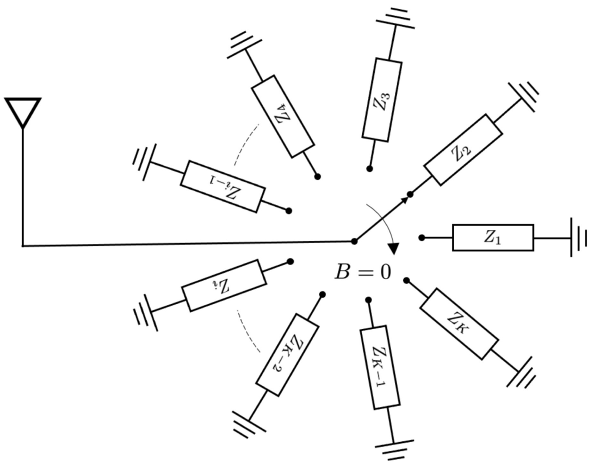

(b) Cycle through phase shifts, i.e., antenna's impedances, anti-clockwise to send a '1'.

FIGURE 2. **The proposed binary tag modulation scheme.**

different loads to cycle through a specific number of fixed phase shifts in one direction (order), while to transmit a '0' bit, the tag will cycle through the same antenna loads but in the opposite direction (order). Implementing these phase shifts is a well-studied problem, originally encountered in the implementation of phase-shift keying in backscatter tags. One implementation in the context of ambient backscatter can be found in [7]. By simply cycling through the phase shifts, we can implement complex sinusoids and unidirectionally shift the spectrum of the ambient signal up or down in frequency. Note that unlike [8], [34], the proposed technique enables unidirectional frequency shifts without sidebands or unwanted frequency components from mixing, and all backscattered energy is retained inside the channel bandwidth, avoiding adjacent channel interference.

The backscattered signal received at the reader can be written as

$$y^b[n] = \begin{cases} \sqrt{\beta^b}\alpha g\, x[n] e^{i2\pi \frac{N}{N_f} n}, & B = 0, \\ \sqrt{\beta^b}\alpha g\, x[n] e^{-i2\pi \frac{N}{N_f} n}, & B = 1. \end{cases} \tag{7}$$

Taking the discrete Fourier transform of (7), the backscattered signal spectrum can be written as

$$Y^b[m] = \begin{cases} \sqrt{\beta^b}\alpha g X[m] \circledast \delta[m-N] = \alpha g\, X[m-N], \ B = 0, \\ \sqrt{\beta^b}\alpha g X[m] \circledast \delta[m+N] = \alpha g\, X[m+N], \ B = 1, \end{cases} \tag{8}$$

where $\circledast$ denotes circular convolution, and $X[m]$ is the discrete Fourier transform (DFT) of $x[n]$. Thus, from the viewpoint of the frequency domain, to transmit a '0' bit, the tag shifts the spectrum of the backscattered signal into the upper guardband, $\mathcal{U}$, while to send a '1', the tag shifts the spectrum of the backscattered signal into the lower guardband, $\mathcal{L}$.

B. DETECTOR

In practice, the ambient backscatter receiver will not have knowledge of the ambient OFDM signal, $s[n]$ or any of the relevant channels, $h[n]$, $f[n]$, or g. Hence, we will have to resort to noncoherent detection. In the case of noncoherent FSK, the square-law detector is actually known to be optimal [35]. Different from energy detection based schemes in [21], [23], this detector does not rely on a threshold and does not need to estimate the average SNR. The proposed detector requires the receiver to only have knowledge of the set of upper and lower guard subcarriers. Moreover, we will show that it has symmetric error probabilities for '0's and '1's, which is another major advantage over energy detection based schemes.

Let $Y[m]$ denote the output of the FFT at the receiver. Then we can write two test statistics, one for the upper guardband, $\mathcal{U}$, as

$$E_u = \frac{2}{\sigma_w^2} \sum_{m \in \mathcal{U}} |Y[m]|^2, \tag{9}$$

and one for the lower guardband, $\mathcal{L}$, as

$$E_l = \frac{2}{\sigma_w^2} \sum_{m \in \mathcal{L}} |Y[m]|^2. \tag{10}$$

Based on these test statistics, we can readily write our detection rule as

$$\hat{B} = \begin{cases} 0, \ E_u > E_l, \\ 1, \ E_l \geq E_u. \end{cases} \tag{11}$$

Since the direct link signal exists only on the data subcarriers, neither E_u nor E_l suffers from direct link interference. Note that, contingent on the transmitted bit, E_u and E_l may depend on the random backscatter channels, $h[n]$ and g. Next, we analyze the distribution of the test statistics and the received SNR.

Let $\mathcal{H}_0$ and $\mathcal{H}_1$ denote the hypotheses that the transmitted bit is '0' or '1', respectively. We first focus on $\mathcal{H}_0$, the hypothesis that the transmitted bit is a '0'. Under $\mathcal{H}_0$, the backscattered signal spectrum is shifted into the upper guardband subcarriers, $\mathcal{U}$, and the lower guardband subcarriers, $\mathcal{L}$, contain only noise. Hence, E_l is just the sum of the squares of N standard Gaussian random variables. Hence, $E_l|\mathcal{H}_0 \sim \chi^2_{2N}$, where χ^2_{2N} denote the central chi-squared variate with $2N$ degrees of freedom. On the other hand, E_u depends on the random backscatter channel. The instantaneous received signal-to-noise ratio in the upper guardband can be written as

$$\gamma_u = \frac{\rho\beta^b|\alpha|^2|g|^2\sum_{m\in\mathcal{U}}|H[m]|^2}{N\sigma_w^2}, \tag{12}$$

where $\{H[m]\}_{m\in\mathcal{U}}$ are the flat-fading channel coefficients seen by the upper guardband subcarriers. Hence, conditional on the instantaneous received SNR, $E_u|\mathcal{H}_0 \sim \chi^2_{2N}(2N\gamma_u)$ where $\chi^2_{2N}(2N\gamma_u)$ is the noncentral chi-squared distribution with $2N$ degrees of freedom and noncentrality parameter $2N\gamma_u$.

Under $\mathcal{H}_1$, the backscattered signal spectrum is shifted to the lower guardband subcarriers, $\mathcal{L}$, and we have a reciprocal situation to that under $\mathcal{H}_0$. In particular, E_u is just the sum of the squares of N standard Gaussian random variables and follows the central chi-squared distribution, i.e., $E_u|\mathcal{H}_1 \sim \chi^2_{2N}$. While E_l depends on the instantaneous received SNR in the lower guardband subcarriers, which can be written as

$$\gamma_l = \frac{\rho\beta^b|\alpha|^2|g|^2\sum_{m\in\mathcal{L}}|H[m]|^2}{N\sigma_w^2}, \tag{13}$$

where $\{H[m]\}_{m\in\mathcal{L}}$ are the flat-fading channel coefficients seen by the lower guardband subcarriers. Hence, conditional on the instantaneous received SNR, $E_l|\mathcal{H}_1 \sim \chi^2_{2N}(2N\gamma_l)$.

Note that since $\{H[m]\}_{m\in\mathcal{U}}$ and $\{H[m]\}_{m\in\mathcal{L}}$ are identically distributed, the instantaneous received SNRs in the upper and lower guard subcarriers, γ_u and γ_l, are also identically distributed. From now on, we denote the instantaneous received SNR in either band by γ.

The instantaneous SNR, γ, is a scaled product of two random variables: $|g|^2$, which is an exponential random variable, and $q \triangleq \sum_{m\in\mathcal{U}}|H[m]|^2$ (or equivalently $\sum_{m\in\mathcal{L}}|H[m]|^2$), which is the sum of N *correlated* exponential random variables. The correlation arises from the fact that the subcarrier spacing has to be smaller than the coherence bandwidth. Let $\mathbf{h}$ denote the vector comprising the channel coefficients $\{H[m]\}_{m\in\mathcal{U}}$ (or $\{H[m]\}_{m\in\mathcal{L}}$). Then, using the technique in [36], the distribution of q can be found to be

$$p(q) = \sum_{j=1}^{J}\left(\prod_{k\neq j}\frac{\frac{1}{\lambda_k}}{\frac{1}{\lambda_k}-\frac{1}{\lambda_j}}\right)\frac{1}{\lambda_j}e^{-\frac{q}{\lambda_j}}, \tag{14}$$

where $\{\lambda_r\}_{r=j}^{J}$ are the non-zero eigenvalues of the co-variance matrix $E[\mathbf{h}\mathbf{h}^{\dagger}]$. Using the product distribution formula, the instantaneous SNR distribution can be readily found to be

$$p(\gamma) = \sum_{j=1}^{J}\left(\prod_{k\neq j}\frac{\frac{1}{\lambda_k}}{\frac{1}{\lambda_k}-\frac{1}{\lambda_j}}\right)\frac{2N}{\lambda_j\overline{\gamma}}\mathbf{K}_0\left(2\sqrt{\frac{N}{\lambda_j}\frac{\gamma}{\overline{\gamma}}}\right), \tag{15}$$

where $\overline{\gamma} \triangleq E[\gamma] = |\alpha|^2\frac{\rho}{\sigma_w^2}$ is the average detection SNR and $\mathbf{K}_m(\cdot)$ is the modified Bessel function of the second kind and m-th order.

C. ERROR PERFORMANCE

Next, we analyze the probability of error for the proposed scheme. Assuming the tag transmitted bits are equally probable to be ones or zeros, the probability of error is given by

$$P_e = \frac{1}{2}\Big[P\Big(\hat{B}=1|\mathcal{H}_0\Big) + P\Big(\hat{B}=0|\mathcal{H}_1\Big)\Big], \tag{16}$$

which is equivalent to

$$\begin{aligned} P_e &= \frac{1}{2}[P(E_l > E_u|\mathcal{H}_0) + P(E_u > E_l|\mathcal{H}_1)] \\ &= \frac{1}{2}\left[P\left(\frac{E_l}{E_u} < 1|\mathcal{H}_0\right) + P\left(\frac{E_u}{E_l} < 1|\mathcal{H}_1\right)\right]. \end{aligned} \tag{17}$$

Note that $E_l|\mathcal{H}_0 \overset{d}{=} E_u|\mathcal{H}_1$ and $E_l|\mathcal{H}_1 \overset{d}{=} E_u|\mathcal{H}_0$, where $\overset{d}{=}$ denotes equality in distribution. Hence, unlike energy detection based techniques [21], [23], which have different false-alarm and missed-detection probabilities at the optimal threshold leading to asymmetric error performance, we have symmetric error probabilities under $\mathcal{H}_0$ and $\mathcal{H}_1$.

Since we have symmetric error probabilities, it is sufficient to find the error probability under $\mathcal{H}_0$. We already discussed the distribution of E_l and E_u in the previous subsection. Under $\mathcal{H}_0$, and conditional on the channel, E_l follows a noncentral chi-squared distribution with noncentrality parameter $2N\gamma$ and E_u follows a central chi-squared distribution, both with $2N$ degrees of freedom. Since E_l and E_u are independent, the quotient $z \triangleq \frac{E_l}{E_u}$ follows the Fisher-Snedecor *singly* noncentral F-distribution [37] whose probability density function is given by

$$p(z) = \sum_{j=0}^{\infty}\frac{e^{\delta/2}(\delta/2)}{B(\frac{v_2}{2},\frac{v_1}{2}+j)j!}\left(\frac{v_1}{v_2}\right)^{\frac{v_1}{2}+j}\left(\frac{v_2}{v_2+v_1z}\right)^{\frac{v_1+v_2}{2}+j}z^{\frac{v_1}{2}-1+j}, \tag{18}$$

where $B(\cdot,\cdot)$ is the beta function [38], v_1 and v_2 are the degrees of freedom of the numerator and denominator, respectively, and δ is the noncentrality parameter of the numerator. The cumulative distribution function is given by

$$F(z;v_1,v_2,\delta) = \sum_{\ell=0}^{\infty}\left(\frac{\left(\frac{\delta}{2}\right)^{\ell}}{\ell!}e^{-\frac{\delta}{2}}\right)I\left(\frac{v_1z}{v_2+v_1z}|\frac{v_1}{2}+\ell,\frac{v_2}{2}\right), \tag{19}$$

where $I(x|a,b)$ is the *incomplete* beta function with parameters a and b [38]. Hence, the instantaneous probability of error can be written as

$$P_e = F(1; 2N, 2N, 2N\gamma) = \sum_{\ell=0}^{\infty}\left(\frac{(N\gamma)^{\ell}}{\ell!}e^{-N\gamma}\right)I\left(\frac{1}{2}|N+\ell, N\right). \tag{20}$$

To get the average probability of error, we need to average the error probability in (20) over the distribution of the SNR obtained in (15). Expressing the exponential and Bessel functions in terms of the Meijer G-function [38], we can write the average probability of error as

$$\overline{P_e} = \sum_{\ell=0}^{\infty}\sum_{j=0}^{J}\frac{N^{\ell}}{\ell!}I\left(\frac{1}{2}|N+\ell, N\right)\left(\prod_{k\neq j}\frac{\frac{1}{\lambda_k}}{\frac{1}{\lambda_k}-\frac{1}{\lambda_j}}\right) \times \int_0^{\infty}\gamma^{\ell-1}G_{0,1}^{1,0}\left({-\atop 0}\middle|N\gamma\right)G_{0,2}^{2,0}\left({-\atop 1,1}\middle|\frac{N}{\lambda_j}\frac{\gamma}{\overline{\gamma}}\right)d\gamma. \tag{21}$$

The integral in (21) can be solved with the help of [39, 07.34.21.0011.01] to obtain the final expression for the average error probability of error as

$$\overline{P_e} = \sum_{\ell=0}^{\infty}\sum_{j=0}^{J}\left(\prod_{k\neq j}\frac{\frac{1}{\lambda_k}}{\frac{1}{\lambda_k}-\frac{1}{\lambda_j}}\right)\frac{I\left(\frac{1}{2}|N+\ell, N\right)}{\ell!} \times G_{1,2}^{2,1}\left({1-\ell \atop 1,1}\middle|\frac{1}{\lambda_j\,\overline{\gamma}}\right). \tag{22}$$

Both the incomplete beta function and the Meijer G-function are available as built-in functions in MATLAB, making the evaluation of this expression straight-forward.

IV. FOUR-ARY MODULATION

In this section, we propose a 4-ary frequency shift keying modulation technique for backscatter communications over ambient OFDM signals. The proposed scheme doubles the maximum transmission rate while maintaining all the advantages of the binary scheme proposed in the preceding section. In particular, it allows easy detection without computing cumbersome SNR-dependent thresholds, and it benefits from symmetrical error performance, which gives equal error protection to all transmitted symbols. We describe the tag modulation waveform and study the optimal noncoherent detector. We also analyze the error performance of the proposed scheme and obtain an analytical bound for the average error probability that is later shown to be sufficiently tight in the simulation results.

A. FOUR-ARY FSK BACKSCATTER WAVEFORM

Similar to the binary scheme presented in Section III, the proposed 4-ary scheme also makes use of in-band null subcarriers along the two sides of the spectrum. The number of those subcarriers will depend on the channel bandwidth and the subcarriers spacing. In particular, the tag modulation waveform selectively shifts the spectrum of the backscattered signal to specific dis-joint subsets of either the upper or lower guardbands to transmit two bits of information. In particular, we divide the upper and lower guardbands into two equal subsets, each of cardinality $\frac{N}{2}$. The backscatter waveform is then designed such that backscattered energy exist in only one of the four subsets, $\{\mathcal{N}_m\}_{m=1}^{4}$. Fig. 3 illustrates the proposed division of the guardbands into four subsets. Note that different from the proposed M-ary scheme in [30], these subsets are completely dis-joint. A simple square-law noncoherent detector is then used to decode the tag information by finding which subset carries more energy. The detector does not need to know the transmitted OFDM symbol, any of the relevant channels, or even set a detection threshold.

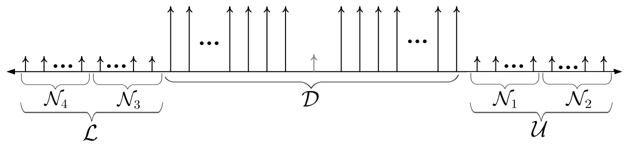

FIGURE 3. Proposed division of the guardbands into four subsets.

Let every backscatter symbol span the duration of one legacy OFDM symbol [21], [28]. The tag uses one of the following four waveforms to convey two information bits per OFDM symbol,

$$b[n] \triangleq \begin{cases} e^{i2\pi\frac{N/2}{N_f}n}, & B = 00, \\ e^{-i2\pi\frac{N/2}{N_f}n}, & B = 01, \\ e^{i2\pi\frac{D+N/2}{N_f}n}, & B = 10, \\ e^{-i2\pi\frac{D+N/2}{N_f}n}, & B = 11, \end{cases} \tag{23}$$

where $n = 1, 2, \ldots, N_f + N_{cp}$, D denotes the number of data subcarriers, i.e., $|\mathcal{D}|$, and $B \in \{00, 01, 10, 11\}$ is the information bits being transmitted. As in the binary case, these waveforms can be implemented by cycling through different antenna loads. However, two different sets of phase shifts are needed. The specific phase shifts set and the direction (order) at which the phase shifts are applied specifies which waveform is transmitted. This modulation scheme is straight-forward to implement in a backscatter tag with limited complexity. It is worth mentioning that it assumed that any energy backscattered outside of the channel bandwidth is cut-off by the receiving filter. This will not cause discernible interference to adjacent channels, as the passively backscattered signal is much weaker than ambient active transmission.

B. FOUR-ARY DETECTOR

The optimal noncoherent detector is a simple square-law detector. Recall, $Y[m]$ denotes the output of the FFT at the receiver. We construct the following four test statistics, one for each subset as

$$E_{\mathsf{m}} = \frac{2}{\sigma_w^2}\sum_{m\in\mathcal{N}_{\mathsf{m}}}|Y[m]|^2, \qquad \mathsf{m} = 1, 2, 3, 4. \tag{24}$$

Hence, the optimal noncoherent detector can be written as

$$\hat{\mathsf{m}} = \arg\max_{1\leq\mathsf{m}\leq M} E_{\mathsf{m}}, \tag{25}$$

C. ERROR PERFORMANCE

Assuming all symbols are equiprobable, the probability of symbol error can be written as

$$P_e = \frac{1}{M}\sum_{\mathrm{m}=1}^{M} P_{e|\mathcal{H}_{\mathrm{m}}}, \tag{26}$$

where $P_{e|\mathcal{H}_m}$ denote the probability of error given the m-th symbol has been transmitted. Owing to the symmetric nature of the scheme, it is sufficient to consider the hypothesis $\mathcal{H}_1$. In this case, E_1 follows a non-central chi-squared distribution and the remaining test statistics all follow a central chi-squared distribution. The probability of making a correct decision can be written as

$$\begin{aligned} P_e &= P_{e|\mathcal{H}_1} = 1 - P_{c|\mathcal{H}_1}, \\ &= 1 - \Pr[E_2 < E_1, E_3 < E_1, E_4 < E_1], \\ &= 1 - \int_0^\infty (\Pr[E_2 < \epsilon])^3 f_{E_1}(\epsilon) d\epsilon, \end{aligned} \tag{27}$$

where P_c is the probability of making a correct decision. Then, substituting the CDF of the central chi-squared distribution and the pdf of the non-central chi-squared distribution gets us

$$P_e = 1 - \int_0^\infty \frac{1}{2}\left(P\left(\frac{N}{2}, \frac{\epsilon}{2}\right)\right)^3 e^{\frac{\epsilon + N\gamma}{2}} \left(\frac{\epsilon}{N\gamma}\right)^{\frac{N}{4}-\frac{1}{2}} I_{\frac{N}{2}-1}\left(\sqrt{N\gamma\epsilon}\right) d\epsilon, \tag{28}$$

where $P(\cdot,\cdot)$ denotes the regularized gamma function [38]. To the best of our knowledge, this integral does not have a closed-form solution; hence, a closed-form expression for the probability of error is intractable, even conditional on the channels. However, a union bound can be derived. Define the pair-wise probability of error, $P_{\mathrm{m}\to\dot{\mathrm{m}}}$, as

$$P_{\mathrm{m}\to\dot{\mathrm{m}}} = \frac{1}{2}\left[P\left(E_{\dot{\mathrm{m}}} > E_{\mathrm{m}} | \mathcal{H}_{\mathrm{m}}\right) + P\left(E_{\mathrm{m}} > E_{\dot{\mathrm{m}}} | \mathcal{H}_{\dot{\mathrm{m}}}\right)\right]. \tag{29}$$

The pairwise error probability expression is identical to the probability of error of the binary scheme, cf. (17), and a closed-form expression for it can be obtained following the steps outlined in Section III. In particular, the average pairwise error probability can be written as

$$P_{\mathrm{m}\to\dot{\mathrm{m}}} = \sum_{\ell=0}^{\infty}\sum_{j=0}^{J}\left(\prod_{k\neq j}\frac{\frac{1}{\lambda_k}}{\frac{1}{\lambda_k}-\frac{1}{\lambda_j}}\right)\frac{I\left(\frac{1}{2}|\frac{N}{2}+\ell, \frac{N}{2}\right)}{\ell!} G_{1,2}^{2,1}\left(\begin{smallmatrix}1-\ell \\ 1,1\end{smallmatrix}\middle|\frac{1}{\lambda_j\,\overline{\gamma}}\right). \tag{30}$$

The pairwise error probability can be used to bound the symbol error probability as

$$P_e \leq \frac{1}{M}\sum_{\mathrm{m}=1}^{M}\sum_{\substack{1\leq\dot{\mathrm{m}}\leq M \\ \dot{\mathrm{m}}\neq\mathrm{m}}} P_{\mathrm{m}\to\dot{\mathrm{m}}}. \tag{31}$$

Simulation results presented later in Section VI will demonstrate the proposed bound is valid and sufficiently tight.

V. MULTI-ANTENNA RECEIVER

In this section, we investigate the use of multiple antennas at the reader to improve error performance. Multi-antenna reception can be used for both binary and 4-ary modulations. We consider noncoherent combining since the reader does not possess channel information. We derive the distribution of the SNR at the output of the combiner and analyze the error performance. Assume the receiver has R antennas and let $Y_r[m]$ denote the output of the FFT at the r-th receive antenna.

A. BINARY MODULATION

Given the difficulty of obtaining channel information at the reader, a noncoherent combining technique is preferable. Hence, we use noncoherent post-detection EGC, i.e., square-law combining, which is known to be optimal for FSK [40]. For this combining technique, the received energy is simply added over all receive antennas. For the binary modulation schemes, two test statistics are constructed, one for the upper guardband and one for the lower guardband. Denote the combined test statistic at the upper guardband by

$$E_u^{\text{comb.}} = \frac{2}{\sigma_w^2}\sum_{r=1}^{R}\sum_{m\in\mathcal{U}}|Y_r[m]|^2, \tag{32}$$

and at the lower guardband by

$$E_l^{\text{comb.}} = \frac{2}{\sigma_w^2}\sum_{r=1}^{R}\sum_{m\in\mathcal{L}}|Y_r[m]|^2. \tag{33}$$

Using the combined test statistics, we can construct the detection rule similar to the single-antenna case as

$$\hat{B} = \begin{cases} 0, & E_u^{\text{comb.}} > E_l^{\text{comb.}}, \\ 1, & E_l^{\text{comb.}} \geq E_u^{\text{comb.}}. \end{cases} \tag{34}$$

Note that the multi-antenna receiver retains all the advantages of the single-antenna receiver. In particular, neither $E_u^{\text{comb.}}$ nor $E_l^{\text{comb.}}$ suffer from direct link interference, there is no need for an SNR specific detection threshold, and the probability of error is symmetric. Next, we look into the distribution of the combined test statistics and the probability of error.

Similar to the single-antenna receiver, the distribution of the test statistics is symmetric under $\mathcal{H}_0$ and $\mathcal{H}_1$. In particular, $E_u^{\text{comb.}}|\mathcal{H}_0 \overset{d}{=} E_l^{\text{comb.}}|\mathcal{H}_1$ and $E_l^{\text{comb.}}|\mathcal{H}_0 \overset{d}{=} E_u^{\text{comb.}}|\mathcal{H}_1$, where $\overset{d}{=}$ denotes equality in distribution. Owing to this symmetry, it is sufficient to consider the hypothesis that the transmitted bit is a '0', i.e., $\mathcal{H}_0$. Under $\mathcal{H}_0$, the backscattered spectrum is shifted to the upper guardband, $\mathcal{U}$, and the lower guardband contains only noise. Hence, $E_l^{\text{comb.}}|\mathcal{H}_0$ is the sum of absolute values of RN standard complex Gaussian random variables, which is independent of the relevant channels, and follows a central chi-squared distribution with $2RN$ degrees of freedom, i.e., $E_l^{\text{comb.}}|\mathcal{H}_0 \sim \chi^2_{2RN}$. In contrast, $E_u^{\text{comb.}}|\mathcal{H}_0$ depends on the relevant channels through the instantaneous SNR at the output of the combiner. Let $\gamma_u^{\text{comb.}}$ denote the instantaneous SNR at the output of the combiner for the upper guardband, which can be written as

$$\gamma_u^{\text{comb.}} = \frac{\rho}{N\sigma_w^2}\sum_{r=1}^{R}|g_r|^2 \sum_{m\in\mathcal{U}}|H[m]|^2, \tag{35}$$

where g_r denotes the channel between the tag and the r-th receive antenna. The distribution of this form of SNR can be found to be [30]

$$p\left(\gamma_u^{\text{comb.}}\right) = \frac{\left(\gamma_u^{\text{comb.}}\right)^{-1}}{(R-1)!}\sum_{j=1}^{J}\left(\prod_{k\neq j}\frac{\frac{1}{\lambda_k}}{\frac{1}{\lambda_k}-\frac{1}{\lambda_j}}\right) G_{0,2}^{2,0}\left(\begin{matrix}-\\ R,1\end{matrix}\middle|\frac{|\mathcal{U}|\gamma_u^{\text{comb.}}}{\lambda_j\overline{\gamma}}\right). \tag{36}$$

Note that the distribution of the SNR for the lower guardband, $\gamma_l^{\text{comb.}}$, is identical. In the sequel, we denote both SNRs by $\gamma^{\text{comb.}}$ for notational convenience. Conditional on the SNR, $E_u^{\text{comb.}}|\mathcal{H}_0$ follows a non-central chi-squared distribution with $2RN$ degrees of freedom and noncentrality parameter $2RN\gamma^{\text{comb.}}$, i.e., $E_u^{\text{comb.}}|\mathcal{H}_0 \sim \chi^2_{2RN}(2RN\gamma^{\text{comb.}})$. Next, we analyze the error performance of the proposed multi-antenna receiver.

1) ERROR PERFORMANCE

Assuming the tag transmitted bits are equally probable to be ones or zeros, the probability of error for the multi-antenna receiver, conditional on the instantaneous SNR, is given by

$$P_e = \frac{1}{2}\left[P\left(\hat{B}=1|\mathcal{H}_0\right)+P\left(\hat{B}=0|\mathcal{H}_1\right)\right], \tag{37}$$

which is equivalent to

$$\begin{aligned}P_e &= \frac{1}{2}\left[P\left(E_l^{\text{comb.}} > E_u^{\text{comb.}}|\mathcal{H}_0\right)+P\left(E_u^{\text{comb.}} > E_l^{\text{comb.}}|\mathcal{H}_1\right)\right]\\ &= \frac{1}{2}\left[P\left(\frac{E_l^{\text{comb.}}}{E_u^{\text{comb.}}}<1|\mathcal{H}_0\right)+P\left(\frac{E_u^{\text{comb.}}}{E_l^{\text{comb.}}}<1|\mathcal{H}_1\right)\right].\end{aligned} \tag{38}$$

This expression is similar to the one obtained in III when a single-antenna receiver is used. In particular, the instantaneous probability of error can be written using the CDF of the Fisher-Snedecor *singly* noncentral F-distribution as

$$\begin{aligned}P_e &= F\left(1; 2RN, 2RN, 2N\gamma^{\text{comb.}}\right)\\ &= \sum_{\ell=0}^{\infty}\left(\frac{\left(N\gamma^{\text{comb.}}\right)^{\ell}}{\ell!}e^{-N\gamma^{\text{comb.}}}\right)I\left(\frac{1}{2}|RN+\ell, RN\right).\end{aligned} \tag{39}$$

To get the average probability of error, we average the above expression over the distribution of the instantaneous SNR at the output of the combiner, $f(\gamma^{\text{comb.}})$, to get

$$\begin{aligned}\overline{P_e} &= \frac{1}{(R-1)!}\sum_{\ell=0}^{\infty}\sum_{j=0}^{J}\frac{N^{\ell}}{\ell!}I\left(\frac{1}{2}|RN+\ell, RN\right)\left(\prod_{k\neq j}\frac{\frac{1}{\lambda_k}}{\frac{1}{\lambda_k}-\frac{1}{\lambda_j}}\right)\\ &\times\int_0^{\infty}\gamma^{\ell-1}G_{0,1}^{1,0}\left(\begin{matrix}-\\0\end{matrix}|N\gamma\right)G_{0,2}^{2,0}\left(\begin{matrix}-\\R,1\end{matrix}\middle|\frac{N\gamma}{\lambda_j\overline{\gamma}}\right)d\gamma,\end{aligned} \tag{40}$$

which can be evaluated similarly to the single-antenna receiver to finally get

$$\overline{P_e} = \frac{1}{(R-1)!}\sum_{\ell=0}^{\infty}\sum_{j=0}^{J}\left(\prod_{k\neq r}\frac{\frac{1}{\lambda_k}}{\frac{1}{\lambda_k}-\frac{1}{\lambda_j}}\right)\frac{I\left(\frac{1}{2}|N+\ell, N\right)}{\ell!} G_{1,2}^{2,1}\left(\begin{matrix}1-\ell\\R,1\end{matrix}\middle|\frac{1}{\lambda_j\overline{\gamma}}\right). \tag{41}$$

B. 4-ARY MODULATION

The same multi-antenna noncoherent combining technique can be applied to the 4-ary modulation as well. In particular, the four test statistics can be constructed as

$$E_{\mathsf{m}}^{\text{comb.}} = \frac{2}{\sigma_w^2}\sum_{r=1}^{R}\sum_{m\in\mathcal{N}_{\mathsf{m}}}|Y_r[m]|^2, \qquad \mathsf{m}=1,2,3,4, \tag{42}$$

and the optimal decision rule can be written as

$$\hat{\mathsf{m}} = \arg\max_{1\leq\mathsf{m}\leq M} E_{\mathsf{m}}^{\text{comb.}}. \tag{43}$$

1) ERROR PERFORMANCE

Similar to the single-antenna receiver, a union bound can be used to characterize the error performance analytically. We only need to compute the pairwise error probability when a multi-antenna receiver is used. Using the distribution of the instantaneous SNR at the output of the combiner and following the same steps as in Section III, we can readily arrive at

$$P_{\mathsf{m}\to\hat{\mathsf{m}}} = \frac{1}{(R-1)!}\sum_{\ell=0}^{\infty}\sum_{j=0}^{J}\left(\prod_{k\neq j}\frac{\frac{1}{\lambda_k}}{\frac{1}{\lambda_k}-\frac{1}{\lambda_j}}\right)\frac{I\left(\frac{1}{2}|\frac{N}{2}+\ell, \frac{N}{2}\right)}{\ell!} G_{1,2}^{2,1}\left(\begin{matrix}1-\ell\\R,1\end{matrix}\middle|\frac{1}{\lambda_j\overline{\gamma}}\right), \tag{44}$$

which can be used to bound the error probability as in (31).

VI. RESULTS AND DISCUSSION

In this section, we evaluate the performance of the proposed scheme by numerical Monte-Carlo simulations and verify the analysis carried out in the preceding sections. As specified in earlier sections, all channels are assumed to be mutually independent multipath Rayleigh fading channels and path-loss attenuation is subsumed in the average signal-to-noise ratio, $\overline{\gamma}$. In our simulations, we use the OFDM system parameters from the LTE standard. We study the effects of the OFDM symbol size and maximum channel delay spread, τ, on the error performance. Moreover, we compare our proposed scheme against the baseline energy detection based scheme from [23], which has been shown to outperform the other energy detection based scheme in [21].

The scheme in [23] also makes use of the guardband subcarriers along the edges of the OFDM symbol spectrum. In particular, to send a '1', the tag switches its antenna impedance between two states, causing the spectrum of the backscattered signal to fall on both sides of the guardband.

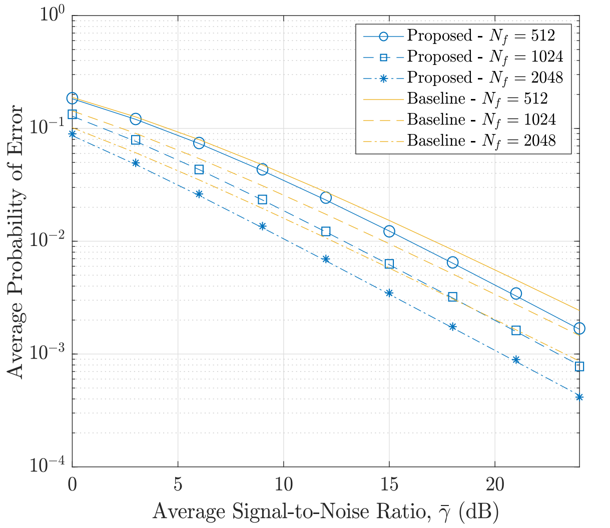

FIGURE 4. **Average probability of error for different OFDM carrier bandwidths, and a maximum channel delay spread, τ, of 3 μs. Lines correspond to Monte-Carlo simulations and markers correspond to analytical expressions. Baseline scheme from [23] is simulated.**

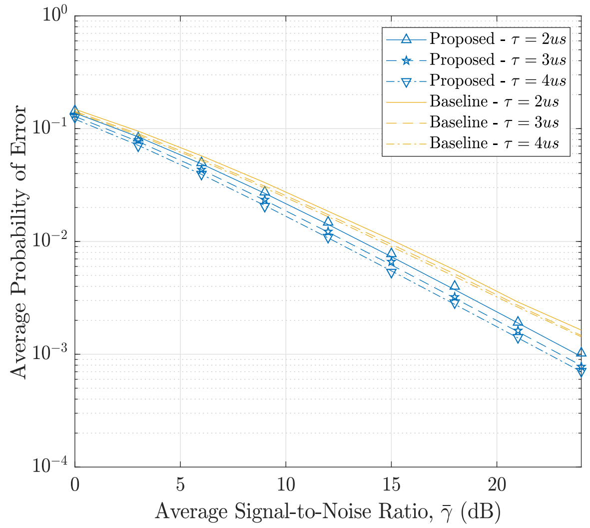

FIGURE 5. **Average probability of error for different values of τ. Lines correspond to Monte-Carlo simulations and markers correspond to analytical expressions. Baseline scheme from [23] is simulated. $N_f = 1024$.**

TABLE 1. **OFDM symbol sizes.**

Symbol Size	Inband Null Subcarriers
N_f	N
512	16
1024	32
2048	64

Whereas to send '0', the tag keeps its antenna impedance constant. Hence, energy detection over the entire guardband can be used to decode the tag information. Drawbacks of that scheme are; first, the energy detector threshold will be a function of the SNR, which needs to be estimated at the receiver; second, the ML detector has asymmetrical error probabilities for '0's and '1's.

In Fig. 4, we vary the OFDM symbol size, N_f, and compare the average bit-error rate of the proposed binary scheme against the baseline from [23] with perfect threshold estimation. The OFDM symbol size, N_f, is representative of the total system bandwidth and the number of in-band null subcarriers on each side of the spectrum, N, increases as N_f increases. In our simulations, we use example N_f, and N values from the LTE standard for 5, 10 and 20MHz carriers. Table 1 shows the relationship between the symbol size and the size of the number of inband null subcarriers. We observe that the proposed scheme outperforms the baseline for all OFDM symbol sizes. This is expected as noncoherent FSK performs better than simple energy detection. Notably, the performance advantage also seems to increase with SNR. For example, note that for $N_f = 2048$, the proposed scheme outperforms the baseline by around 2 dB at a bit-error rate of 10^{-2}, and that advantage grows to more than 3 dB at a bit-error rate of 10^{-3}. We also observe that the error probability obtained from analytical expressions, denoted by markers,

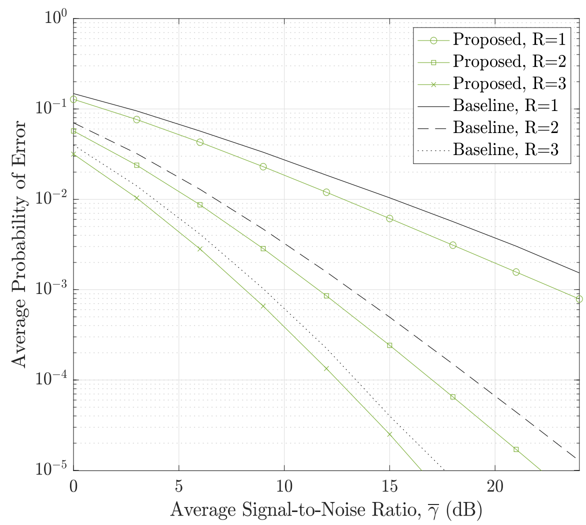

FIGURE 6. **Average probability of error for proposed scheme with multi-antenna reception. Lines correspond to Monte-Carlo simulations and markers correspond to analytical expressions. Baseline scheme from [23]. $N_f = 1024$ and $\tau = 3$ μs.**

matches the simulation results, which verifies our analysis in Section III.

In Fig. 5, we vary the maximum channel delay spread, τ, and compare the probability of error for the proposed binary scheme against the baseline. From the figure, the proposed scheme outperforms the baseline for all values of delay spread. Moreover, the proposed scheme does not seem to be greatly affected by the change in the delay spread, unlike [21] which relies on the remaining part of the cyclic prefix and fails for high values of delay spread. Again, note that the analytical probability of error, denoted by markers, matches the one obtained by simulations, verifying our analysis.

In Fig. 6, we show the performance of the multi-antenna receiver for a different number of antennas and compare it against the baseline from [23]. From the figure, the

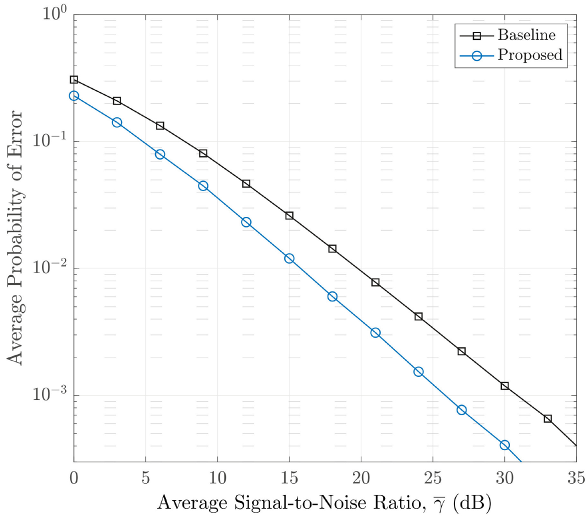

FIGURE 7. **Average probability of error for proposed 4-ary scheme with single-antenna reception. Baseline scheme from [30] shown for comparison. $N_f = 2048$, $\tau = 3\ \mu$s, $R = 1$.**

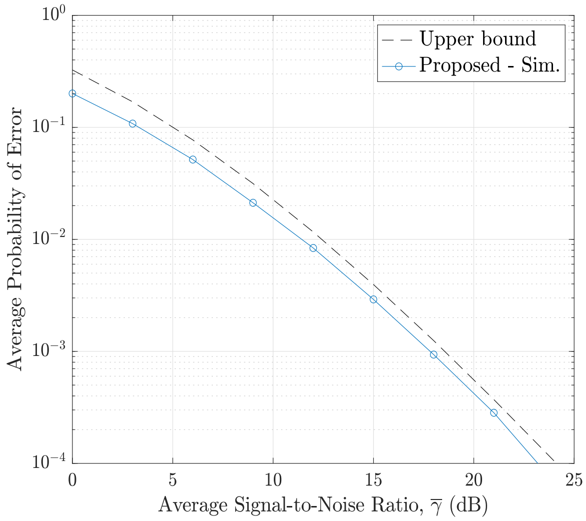

FIGURE 8. **Average probability of error for proposed 4-ary scheme compared to the derived union bound. $N_f = 1024$, $\tau = 3\ \mu$s, $R = 2$.**

performance of the proposed scheme improves significantly by adding multiple receive antennas. However, adding more antenna start to yield diminishing returns, which is expected. The simulated results agree with analytical expressions, which verifies our analysis. Moreover, the proposed scheme outperforms the baseline for all number of antennas simulated.

Next, in Fig. 7, we compare the proposed 4-ary to that from [30]. The 4-ary scheme in [30] also shifts the backscattered to subsets of the guardbands; however, it uses a less sophisticated frequency shifting technique, which leads the subsets to overlap, and detection necessitates a special energy detection scheme based on a table [30]. From the figure, the proposed scheme outperforms by a substantial 5 dB at an error rate of 10^{-3}.

Finally, we evaluate the accuracy of the union bound derived for the four-ary modulation scheme. In Fig. 8, we show the average error probability of 4-ary scheme for an OFDM symbol size, N_f of 1024, a maximum delay spread, τ, of 3 μs, and two receive antennas. From the figure, the union bound upper-bounds the average error probability and gets tighter as the SNR increases as expected.

VII. CONCLUSION

We have proposed a novel technique to implement binary frequency shift keying in backscatter systems over ambient OFDM signals. The proposed technique relies on cycling through different phase shifts to allow unidirectional bandpass frequency shifts enabling the implementation of BFSK over ambient OFDM signals. By exploiting the guardband subcarriers and the orthogonality of the OFDM waveform, we have avoided direct-link and adjacent channels' interference. Moreover, we have studied the optimal noncoherent detector and obtained an exact expression for the average probability of error. Furthermore, to increase the tag transmission rate, we have also proposed a 4-ary modulation scheme and analyzed its error performance; while to improve the error performance, we have proposed the use of a simple multi-antenna combining technique and analyzed its performance. The proposed scheme avoids two drawbacks of energy detection based techniques. First, it allows simple threshold-less detection and exempts the reader from estimating the SNR. Second, it has symmetric error probabilities for '1's and '0's. Our simulation results have corroborated our analysis and showed that the proposed scheme outperforms energy detection schemes available in the literature.

REFERENCES

[1] D. M. Dobkin, *The RF in RFID: UHF RFID in Practice*, 2nd ed. Amsterdam, The Netherlands: Newnes, 2012.
[2] C. Boyer and S. Roy, "Backscatter communication and RFID: Coding, energy, and MIMO analysis," *IEEE Trans. Commun.*, vol. 62, no. 3, pp. 770–785, Mar. 2014.
[3] V. Liu, A. Parks, V. Talla, S. Gollakota, D. Wetherall, and J. R. Smith, "Ambient backscatter: Wireless communication out of thin air," in *Proc. ACM SIGCOMM Conf.*, Hong Kong, China, Aug. 2013, pp. 39–50.
[4] X. Lu, D. Niyato, H. Jiang, D. I. Kim, Y. Xiao, and Z. Han, "Ambient backscatter assisted wireless powered communications," *IEEE Wireless Commun.*, vol. 25, no. 2, pp. 170–177, Apr. 2018.
[5] A. N. Parks, A. Liu, S. Gollakota, and J. R. Smith, "Turbocharging ambient backscatter communication," in *Proc. ACM SIGCOMM Conf.*, Chicago, IL, USA, Aug. 2014, pp. 619–630.
[6] B. Kellogg, A. Parks, S. Gollakota, J. R. Smith, and D. Wetherall, "Wi-Fi backscatter: Internet connectivity for RF-powered devices," in *Proc. ACM SIGCOMM Conf.*, Chicago, IL, USA, Aug. 2014, pp. 607–618.
[7] D. Bharadia, K. R. Joshi, M. Kotaru, and S. Katti, "BackFi: High throughput WiFi backscatter," in *Proc. ACM SIGCOMM Conf.*, London, U.K., Aug. 2015, pp. 283–296.
[8] P. Zhang, M. Rostami, P. Hu, and D. Ganesan, "Enabling practical backscatter communication for on-body sensors," in *Proc. ACM SIGCOMM Conf.*, New York, NY, USA, Aug. 2016, pp. 370–383.
[9] V. Iyer, V. Talla, B. Kellogg, S. Gollakota, and J. R. Smith, "Inter-technology backscatter: Towards Internet connectivity for implanted devices," in *Proc. ACM SIGCOMM Conf.*, Florianópolis, Brazil, Aug. 2016, pp. 356–369.

[10] A. Wang, V. Iyer, V. Talla, J. R. Smith, and S. Gollakota, “FM backscatter: Enabling connected cities and smart fabrics,” in *Proc. 14th USENIX Conf. Netw. Syst. Des. Implement.*, Boston, MA, USA, Mar. 2017, pp. 243–258.
[11] Y. Peng et al., “PLoRa: A passive long-range data network from ambient LoRa transmissions,” in *Proc. ACM SIGCOMM Conf.*, Budapest, Hungary, Aug. 2018, pp. 147–160.
[12] G. Vougioukas and A. Bletsas, “Switching frequency techniques for universal ambient backscatter networking,” *IEEE J. Sel. Areas Commun.*, vol. 37, no. 2, pp. 464–477, Feb. 2019.
[13] D. Darsena, G. Gelli, and F. Verde, “Cloud-aided cognitive ambient backscatter wireless sensor networks,” *IEEE Access*, vol. 7, pp. 57399–57414, 2019.
[14] J. Liao, X. Wang, K. Ruttik, R. Jäntti, and D.-T. Phan-Huy, “In-band ambient FSK backscatter communications leveraging LTE cell-specific reference signals,” *IEEE J. Radio Freq. Identif.*, vol. 7, pp. 267–277, 2023.
[15] R. Duan, R. Jäntti, H. Yigitler, and K. Ruttik, “On the achievable rate of bi-static modulated re-scatter systems,” *IEEE Trans. Veh. Technol.*, vol. 66, no. 10, pp. 9609–9613, Oct. 2017.
[16] G. Wang, F. Gao, Z. Dou, and C. Tellambura, “Uplink detection and BER analysis for ambient backscatter communication systems,” in *Proc. IEEE Global Commun. Conf. (GLOBECOM)*, San Diego, CA, USA, Dec. 2015.
[17] Z. Mat, T. Zeng, G. Wang, and F. Gao, “Signal detection for ambient backscatter system with multiple receiving antennas,” in *Proc. IEEE 14th Canadian Workshop Inform. Theory (CWIT)*, St. John’s, NL, Canada, Jul. 2015, pp. 50–53.
[18] J. Qian, F. Gao, G. Wang, S. Jin, and H. Zhu, “Noncoherent detections for ambient backscatter system,” *IEEE Trans. Wireless Commun.*, vol. 16, no. 3, pp. 1412–1422, Mar. 2017.
[19] J. Qian, F. Gao, G. Wang, S. Jin, and H. Zhu, “Semi-coherent detection and performance analysis for ambient backscatter system,” *IEEE Trans. Commun.*, vol. 65, no. 12, pp. 5266–5279, Dec. 2017.
[20] D. T. Hoang, D. Niyato, P. Wang, D. I. Kim, and Z. Han, “Ambient backscatter: A new approach to improve network performance for RF-powered cognitive radio networks,” *IEEE Trans. Commun.*, vol. 65, no. 9, pp. 3659–3674, Sep. 2017.
[21] G. Yang and Y. C. Liang, “Backscatter communications over ambient OFDM signals: Transceiver design and performance analysis,” in *Proc. IEEE Global Commun. Conf. (GLOBECOM)*, Washington, DC, USA, Dec. 2016.
[22] Q. Zhang, H. Guo, Y. Liang, and X. Yuan, “Constellation learning-based signal detection for ambient backscatter communication systems,” *IEEE J. Sel. Areas Commun.*, vol. 37, no. 2, pp. 452–463, Feb. 2019.
[23] M. A. ElMossallamy, Z. Han, M. Pan, R. Jäntti, K. G. Seddik, and G. Y. Li, “Backscatter communications over ambient OFDM signals using null subcarriers,” in *Proc. IEEE Global Commun. Conf. (GLOBECOM)*, Abu Dhabi, UAE, Dec. 2018, pp. 1–6.
[24] M. Nemati, M. Soltani, J. Ding, and J. Choi, “Subcarrier-wise backscatter communications over ambient OFDM for low power IoT,” *IEEE Trans. Veh. Technol.*, vol. 69, no. 11, pp. 13229–13242, Nov. 2020.
[25] T. Hara, R. Takahashi, and K. Ishibashi, “Ambient OFDM pilot-aided backscatter communications: Concept and design,” *IEEE Access*, vol. 9, pp. 89210–89221, 2021.
[26] M. Lopez, N. He, and T. A. Khan, “Designing a bistatic backscatter communications system with OFDM for 6G Internet of Things,” in *Proc. IEEE 98th Veh. Technol. Conf. (VTC-Fall)*, 2023, pp. 1–6.
[27] Y. Peng, Y. Zhang, L. Xiao, Y. Zeng, and T. Jiang, “Exploiting subcarrier redundancy for concurrent OFDM backscatter communication,” *IEEE Wireless Commun. Lett.*, vol. 12, no. 5, pp. 828–832, May 2023.
[28] D. Darsena, G. Gelli, and F. Verde, “Modeling and performance analysis of wireless networks with ambient backscatter devices,” *IEEE Trans. Commun.*, vol. 65, no. 4, pp. 1797–1814, Apr. 2017.
[29] M. A. ElMossallamy, Z. Han, M. Pan, R. Jantti, K. Seddik, and G. Y. Li, “Noncoherent frequency shift keying for ambient backscatter over OFDM signals,” in *Proc. IEEE Int. Conf. Commun.*, Shanghai, China, May 2019, pp. 1–6.
[30] M. A. ElMossallamy, M. Pan, R. Jäntti, K. G. Seddik, G. Y. Li, and Z. Han, “Noncoherent backscatter communications over ambient OFDM signals,” *IEEE Trans. Commun.*, vol. 67, no. 5, pp. 3597–3611, May 2019.
[31] Y. P. E. Wang et al., “A primer on 3GPP narrowband Internet of Things,” *IEEE Commun. Mag.*, vol. 55, no. 3, pp. 117–123, Mar. 2017.
[32] A. Ghosh, J. Zhang, J. G. Andrews, and R. Muhamed, *Fundamentals of LTE*, 1st ed. Upper Saddle River, NJ, USA: Prentice Hall Press, 2010.
[33] G. Yang, Y.-C. Liang, R. Zhang, and Y. Pei, “Modulation in the air: Backscatter communication over ambient OFDM carrier,” *IEEE Trans. Commun.*, vol. 66, no. 3, pp. 1219–1233, Mar. 2018.
[34] J. F. Ensworth and M. S. Reynolds, “Every smart phone is a backscatter reader: Modulated backscatter compatibility with Bluetooth 4.0 low energy (BLE) devices,” in *Proc. IEEE Int. Conf. RFID (RFID)*, San Diego, CA, USA, Apr. 2015, pp. 78–85.
[35] J. Proakis and M. Salehi, *Digital Communications*, 5th ed. New York, NY, USA: McGraw-Hill Educ., 2007.
[36] I. S. Ansari, F. Yilmaz, M. S. Alouini, and O. Kucur, “On the sum of gamma random variates with application to the performance of maximal ratio combining over Nakagami-m fading channels,” in *Proc. IEEE 13th Int. Workshop Signal Process. Adv. Wireless Commun. (SPAWC)*, Çeşme, Turkey, Jun. 2012, pp. 394–398.
[37] S. M. Kay, *Fundamentals of Statistical Signal Processing, Volume II: Detection Theory*, 1st ed. Englewood Cliffs, NJ, USA: Prentice Hall, Feb. 1998.
[38] F. W. J. Olver, D. W. Lozier, R. F. Boisvert, and C. W. Clark, *NIST Handbook of Mathematical Functions*. Cambridge, NY, USA: Cambridge Univ. Press, May 2010.
[39] “The wolfram functions site,” 2024. [Online]. Available: http://functions.wolfram.com
[40] M. K. Simon and M.-S. Alouini, *Digital Communication Over Fading Channels*, 2nd ed. Hoboken, NJ, USA: Wiley-IEEE Press, Dec. 2004.

MOHAMED A. ELMOSSALLAMY (Member, IEEE) received the M.Sc. degree in electronics and communications engineering from The American University in Cairo, Cairo, Egypt, in 2017, and the Ph.D. degree in electrical engineering from the University of Houston, Houston, TX, USA, in 2020. He is currently a Staff Modem Engineer with Qualcomm Inc., Boxborough, MA, USA. He has held engineering internships with Qualcomm Inc.; MediaTek USA Inc., San Jose, CA, USA; and Skylark Wireless, Houston. His current research interests include transceiver design and performance analysis for the Internet of Things, massive MIMO-OFDM systems, intelligent reflecting surfaces, and machine learning for wireless communications. He was the recipient of the 2019 IEEE ComSoc TCGCC Best Conference Paper Award and an NSF INTERN Award in 2018.

MIAO PAN (Senior Member, IEEE) received the B.Sc. degree in electrical engineering from the Dalian University of Technology, Dalian, China, in 2004, the M.A.Sc. degree in electrical and computer engineering from the Beijing University of Posts and Telecommunications, Beijing, China, in 2007, and the Ph.D. degree in electrical and computer engineering from the University of Florida, Gainesville, FL, USA, in 2012. He is currently an Associate Professor with the Department of Electrical and Computer Engineering, University of Houston, Houston, TX, USA. His research interests include cybersecurity, big data privacy, deep learning privacy, cyber–physical systems, and cognitive radio networks. He was the recipient of the NSF CAREER Award in 2014. His work was the recipient of the IEEE Technical Committee on Green Communications and Computing (TCGCC) Best Conference Paper Awards in 2019, and the Best Paper Awards at ICC 2019, VTC 2018, Globecom 2017, and Globecom 2015, respectively. He is the Editor of IEEE OPEN JOURNAL OF VEHICULAR TECHNOLOGY and an Associate Editor of IEEE INTERNET OF THINGS JOURNAL (Area 5: Artificial Intelligence for IoT), and was an Associate Editor of IEEE INTERNET OF THINGS JOURNAL (Area 4: Services, Applications, and Other Topics for IoT) from 2015 to 2018. He has also been serving as a Technical Organizing Committee for several conferences, such as the TPC Co-Chair of Mobiquitous 2019 and ACM WUWNet 2019. He is a member of AAAI and ACM.

RIKU JÄNTTI (Senior Member, IEEE) received the M.Sc. degree (with Distinction) in electrical engineering and the D.Sc. degree (with Distinction) in automation and systems technology from the Helsinki University of Technology (TKK) in 1997 and 2001, respectively. He is a Full Professor of Communications Engineering with Aalto University School of Electrical Engineering, Finland. Prior to joining Aalto University in August 2006, he was a Professor Pro Tem with the Department of Computer Science, University of Vaasa. His research interests include machine-type communications, disaggregated radio access networks, backscatter communications, quantum communications, and radio frequency inference.

KARIM G. SEDDIK (Senior Member, IEEE) received the B.Sc. (Hons.) and M.Sc. degrees in electrical engineering from Alexandria University, Alexandria, Egypt, in 2001 and 2004, respectively, and the Ph.D. degree from the University of Maryland at College Park, College Park, MD, USA, in 2008.

He is currently a Professor with the Electronics and Communications Engineering Department, American University in Cairo (AUC), where he is also an Associate Dean of Graduate Studies and Research with the School of Sciences and Engineering. Before joining AUC, he was an Assistant Professor with Alexandria University. His research interests include applications of machine learning in communication networks, intelligent reflecting surfaces, age of information, cognitive radio communications, and layered channel coding. He was a recipient of the American University in Cairo Faculty Merit Award for Excellence in Research and Creative Endeavors in 2021, the State Encouragement Award in 2016, the State Medal of Excellence in 2017, and the Certificate of Honor from the Egyptian President for being ranked first among all departments in the College of Engineering, Alexandria University, in 2002. He received the Graduate School Fellowship in 2004 and 2005 and the Future Faculty Program Fellowship in 2017 from the University of Maryland at College Park. He also co-authored a conference paper that received the Best Conference Paper Award from the IEEE Communication Society Technical Committee on Green Communications and Computing in 2019. He currently serves as an Editor for the IEEE TRANSACTIONS ON MACHINE LEARNING IN COMMUNICATIONS AND NETWORKING. He has served on the technical program committees for numerous IEEE conferences in the areas of wireless networks and mobile computing.

GEOFFREY YE LI (Fellow, IEEE) is currently a Chair Professor with Imperial College London, U.K. Before joining Imperial College London in 2020, he was a Professor with the Georgia Institute of Technology, USA, for 20 years and a Principal Technical Staff Member with AT&T Labs-Research (previously Bell Labs), Murray Hill, NJ, USA, for five years. He made fundamental contributions to orthogonal frequency-division multiplexing for wireless communications, established a framework on resource cooperation in wireless networks, and introduced deep learning to communications. In these areas, he has published around 700 journal and conference papers in addition to over 40 granted patents. His publications have been cited over 70 000 times with an H-index of 120.

Dr. Li has been listed as a Highly Cited Researcher by Clarivate/Web of Science almost every year. He won the 2024 IEEE Eric E. Sumner Award, the 2019 IEEE ComSoc Edwin Howard Armstrong Achievement Award, and several other awards from IEEE Signal Processing, Vehicular Technology, and Communications Societies. He was elected to Fellow of the Royal Academic of Engineering and IET Fellow for his contributions to signal processing for wireless communications.

ZHU HAN (Fellow, IEEE) received the B.S. degree in electronic engineering from Tsinghua University in 1997, and the M.S. and Ph.D. degrees in electrical and computer engineering from the University of Maryland at College Park in 1999 and 2003, respectively. From 2000 to 2002, he was a Research and Development Engineer with JDSU, Germantown, MD, USA. From 2003 to 2006, he was a Research Associate with the University of Maryland at College Park. From 2006 to 2008, he was an Assistant Professor with Boise State University, Boise, ID, USA. He is currently a John and Rebecca Moores Professor with the Electrical and Computer Engineering Department and the Computer Science Department, University of Houston, Houston, TX, USA. His main research targets on the novel game-theory-related concepts critical to enabling efficient and distributive use of wireless networks with limited resources. His other research interests include wireless resource allocation and management, wireless communications and networking, quantum computing, data science, smart grid, carbon neutralization, and security and privacy. He received an NSF Career Award in 2010, the Fred W. Ellersick Prize of the IEEE Communication Society in 2011, the EURASIP Best Paper Award for the Journal on Advances in Signal Processing in 2015, the IEEE Leonard G. Abraham Prize in the field of Communications Systems (Best Paper Award in IEEE JSAC) in 2016, the IEEE Vehicular Technology Society 2022 Best Land Transportation Paper Award, and several best paper awards in IEEE conferences. He was an IEEE Communications Society Distinguished Lecturer from 2015 to 2018 and an ACM Distinguished Speaker from 2022 to 2025, and has been an AAAS Fellow since 2019 and an ACM Fellow since 2024. He has been a 1% Highly Cited Researcher since 2017 according to Web of Science. He is also the winner of the 2021 IEEE Kiyo Tomiyasu Award (an IEEE Field Award), for outstanding early to mid-career contributions to technologies holding the promise of innovative applications, with the following citation: "for contributions to game theory and distributed management of autonomous communication networks."